# An inside look at tipping mechanisms for a tropical cyclone

John A. Gemmer*, Katherine Slyman†

Over two decades ago, The Intergovernmental Panel on Climate Change introduced the idea of tipping points as "large scale discontinuities in the climate" [1]. While there is no precise mathematical definition of a tipping event, tipping can be thought of as a rapid, and often irreversible, change in the equilibrium state of a dynamical system [2]. In [3] it was proposed that tipping events could be classified according to whether the underlying mathematical mechanism involves, predominantly, a bifurcation (B-tipping), noise induced transitions (N-tipping), or a rate dependent parameter (R-tipping); see also [4–7]. Classically, B-tipping has been used to study subsystems of the climate which are vulnerable to tipping. However, in B-tipping an implicit assumption is that parameters change slowly relative to the intrinsic timescale set by the deterministic dynamics. The validity of this assumption in climate applications is not clear since anthropogenic change has occurred over a much shorter time span (centuries) than the shortest geological time scale (millions of years) [8]. Moreover, in many climate applications the dynamical system is necessarily stochastic and non-autonomous and thus there is need to study how a combination of these mechanisms can also lead to tipping [3].

In [9] we studied these tipping mechanisms for a low-dimensional model of a tropical cyclone. Specifically, this model couples the dynamics of the tangential wind speed of a cyclone to its inner core moisture with, essentially, the potential energy of the storm, wind shear, and the temperature of the ocean serving as parameters. While classic bifurcations occur as these parameters are varied, we found non-intuitive results when considering rate and noise-induced tipping. Specifically, we found that rapid increases in the potential energy of a storm coupled with sufficient wind shear can destabilize a storm. This result is surprising in that while a slow increase of the potential energy results in a more intense storm, if the energy is increased sufficiently rapid the tangential wind speed cannot increase quickly enough and is dissipated by wind shear. We also found in this model that while the stability of cyclones are exceptionally robust to additive random fluctuations, the presence of noise can lead to the rapid formation of a tropical storm. This consequence of the model results from the existence of a center manifold along which the deterministic dynamics is relatively weak. In this article, we summarize the key techniques used in our analysis.

Because of the destruction that tropical cyclones can cause [10], understanding what mechanisms

*Department of Mathematics, Wake Forest University, Winston-Salem, NC 27109, *Email*: gemmerj@math.edu
†Division of Applied Mathematics, Brown University, Providence, RI 02906, *Email*:katherine_slyman@brown.edu

lead to their formation should be of interest to policy makers, risk analysts, and climate scientists. Indeed, a presumed impact of global climate change is the increase in frequency and intensity of tropical cyclones. For example, in 2019 Hurricane Dorian made landfall in the Bahamas as a category 5 hurricane, sustaining winds over 185 miles per hours and it caused an estimated $7 billion in damages, over 400 dead or missing persons, and immeasurable losses to reef and mangroves, which in turn impacted tourism, the fishing industry, and protection from future storms [11]. As a second example, in 2005, Hurricane Katrina struck the gulf coast of Louisiana and was one of the costliest storms on record, causing over $125 billion, and over 1,800 lives lost despite only sustaining winds of 127 mph upon landfall [12].

# 1 Mathematical Model of a Tropical Cyclone

Tropical cyclones are axisymetric vortices that form over warm ocean water in which there is a temperature gradient between the warm ocean and cooler lower atmosphere. In these regions, as warm water evaporates, the resulting warm air mass rises and cools rapidly releasing heat through condensation back into the atmosphere. As the warm air rises, an area of low pressure forms and air begins to move from all directions to fill this void. The air in this region swirls from the Coriolis effect and, due to conservation of angular momentum, eventually forms a rotating air mass around the area of low pressure, i.e., the eye of the storm. In this idealized setting, this process can modeled as a Carnot engine in which the maximum potential velocity of the hurricane, $V_p > 0$ can be obtained by equating the kinetic energy with the theoretical maximum power that could be sustained by the storm [13, 14]. However, in realistic storms, wind shear in the form of strong upper level winds can dissipate the storm structure by displacing warm temperatures above the storm eye.

To study the formation of tropical storms, the model we considered was a stochastic perturbation of a dynamical system developed in [15, 16] and is given in dimensionless form by

$$\begin{aligned} dv &= f(v,m)d\tau + \sigma_1 dW_1 := \left[(1-\gamma)m^3 - (1-\gamma m^3)v^2\right] d\tau + \sigma_1 dW_1, \\ dm &= g(v,m)d\tau + \sigma_2 dW_2 := \left[(1-m)v - cm\right] d\tau + \sigma_2 dW_2, \end{aligned} \tag{1}$$

where we have restricted the dynamics to the physically relevant first quadrant by assuming reflecting boundary conditions on the axes. Here $v = V/V_p \in [0,1]$ is a dimensionless measure of the tangential velocity $V \geq 0$ of the storm relative to a maximum potential velocity $V_p > 0$, $\tau \sim V_p^{-1}t$, $m \in [0,1]$ is the relative humidity in the core of the storm, $W_1, W_2$ are standard Wiener processes, $c = 2.2S/V_p$ is a dimensionless measure of wind shear $S$ relative to $V_p$, and $\sigma_1, \sigma_2 > 0$ are measures of the amplitude of random fluctuations. The dimensionless parameter $\gamma$ is defined by $\gamma = (T_A - T_O)/T_O + \kappa$, where $T_A$, $T_O$ are the temperatures of the lower atmosphere and upper ocean respectively and $\kappa$ is a constant, and thus $\gamma^{-1}$ is a proxy for the temperature of the ocean. In this model, $m$ serves as a source of energy for the storm and if $m = 1$, i.e., the core is fully saturated, the equilibrium velocity is given by $V = V_p$. The wind shear plays the role of friction in the system in the sense that it dissipates energy by pulling moisture from the storm and if $c = 0$ we see that $m = 1, v = 1$ is a stable fixed point, i.e., the storm reaches its full potential intensity (assuming $\sigma_1 = \sigma_2 = 0$).

The deterministic skeleton of Equation (1) contains an asymptotically stable fixed point $\mathcal{O}$ (non-storm state) at the origin. The system also exhibits a saddle-node bifurcation in which a stable node $\mathcal{S}$ (stable storm state) and a saddle $\mathcal{U}$ (unstable storm state) emerge as $c$ and $\gamma$ are varied. Figure 1(a) is a generic phase portrait of this system in a parameter regime in which all three fixed points exist. Figure 1(b) is a "phase diagram" indicating the intensity of the storm state (when it exists) by the velocity component of $\mathcal{S}$. This figure illustrates that this model predicts more intense storms, which are more difficult to dissipate through wind shear, will result from increasing ocean temperatures, i.e., $\gamma \to 0$.

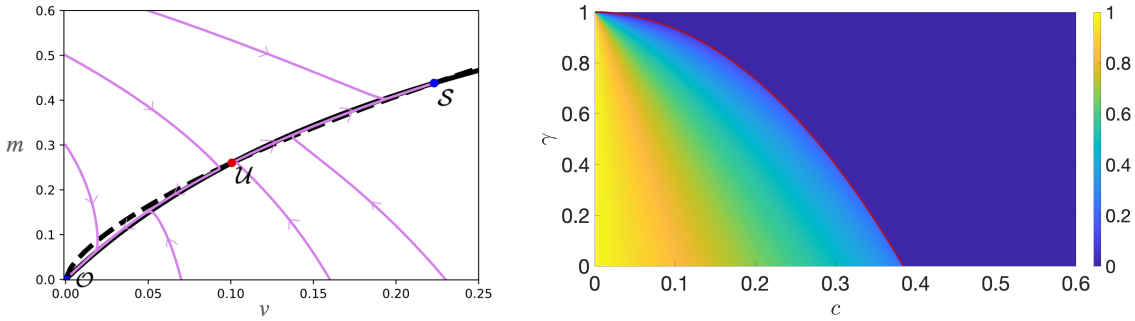


(a) (b)

Figure 1: (a) Phase portrait for Equation (1) with $(c, \gamma) = (.286, .43)$. The blue circles correspond to the stable fixed points $\mathcal{S}$ and $\mathcal{O}$ and the red circle corresponds to the saddle node $\mathcal{U}$. The dashed and solid black lines correspond to the nullclines $\dot{v} = 0$ and $\dot{m} = 0$ respectively. (b) Phase diagram for the deterministic skeleton of Equation (1) in the $(c, \gamma)$ plane. The red curve corresponds to the values of $c, \gamma$ in which saddle node bifurcations occur and divides the $(c, \gamma)$ plane into two regions. The lower left region is colored by the dimensionless velocity of the storm state $\mathcal{S}$ while the upper right region is colored blue to indicate that the only stable fixed is the origin, i.e., the non-storm state.

## 2 Rate-induced tipping

Rate-induced tipping occurs when a quick change of a parameter causes the system to move away from one attractor to another [2]. However, this change of system behavior happens without the system undergoing a bifurcation; fixed points may move through different basins of attraction over a parameter shift, but never cross a bifurcation curve. In particular, it is the rate of change of the parameters not the necessarily the specific changes in the values of the parameters that governs the tipping. In our work, we assumed a parameter shift $\Lambda_r$ that varies at a rate $r > 0$, is bi-asymptotically constant, and is monotonically increasing. Note, since $\mathcal{O}$ is always a fixed point it follows that regardless of parameter values there can be no rate induced tipping away from $\mathcal{O}$. Consequently, we focused on rate induced tipping which could destabilize the storm, i.e., causes the system to move from $\mathcal{S}$ to $\mathcal{O}$.

The conditions for rate-induced tipping to occur are actually the same for any dimension: if the initial state satisfies a sufficient condition called *forward threshold unstable* [17]. Essentially

this condition implies the initial state at the start of the parameter shift lies in the basin of attraction of a different stable state at the end of the parameter shift. However, we note forward threshold stability is not a necessary condition to prevent rate-induced tipping in systems of higher dimension. Indeed, for systems of dimension $n > 1$, the more refined condition of *inflowing stability* guarantees that rate-induced tipping cannot happen [18].

To consider the possibility of rate-induced tipping aiding in the formation or destabilization of a storm, we needed physical parameters with the ability to rapidly change. In the model, both wind shear and maximum potential velocity meet these requirements, and thus we allowed $c$ and $V_p$ to vary with time. As rate-induced tipping is a deterministic mechanism, we set $\sigma_1 = \sigma_2 = 0$ and considered the dimensional system. To do this, we redefined both $V_p$ and $c$ as functions of a parameter shift $\Lambda_r = \frac{1}{2}(1 + \tanh(rt))$. Specifically, we assumed $V_p, c$ to transition in time between $V_p^-$ to $V_p^+$ and $c^-$ to $c^+$, respectively, which represents the minimum and maximum values of the parameters. Additionally, we chose parameter shifts such that there are always three fixed points at the start and end of the ramp which we denote $\mathcal{O}, \mathcal{U}^-, \mathcal{S}^-$ and $\mathcal{O}, \mathcal{U}^+, \mathcal{S}^+$ respectively.

In regard to storm destabilization, we used the condition of inflowing stability to show that if either $V_p(\Lambda_r(\tau))$ or $c(\Lambda_r(\tau))$ is nonincreasing as a function of $\tau$, there can be no rate-induced tipping away from the stable storm state $\mathcal{S}^-$ to the non-storm state $\mathcal{O}$. However, if both $V_p(\Lambda_r(\tau))$, and $c(\Lambda_r(\tau))$ are increasing, then there is the possibility of rate-induced tipping from $\mathcal{S}^-$ to $\mathcal{O}$ for $r$ sufficiently large. This implies both wind shear and maximal potential velocity have to increase at a substantial rate in order to affect tipping away from the active storm state. These results are illustrated by a numerical example in Figure 2. In this example, we chose a parameter shift $\Lambda_r(\tau)$, and increasing functions $V_p$ and $c$ that are dependent on $\Lambda_r(\tau)$ such that $\mathcal{S}^-$ lies in the basin of attraction of $\mathcal{O}$ at the end of the parameter shift, ensuring forward threshold instability; see Figure 2(a). Figure 2(b) illustrates that for $r$ small we endpoint track the stable path from $\mathcal{S}^-$ to $\mathcal{S}^+$, and no tipping occurs but when $r$ is sufficiently large we tip from $\mathcal{S}^-$ to $\mathcal{O}$.

## 3 Noise-induced tipping

A noise-induced tipping event from $\mathcal{O}$ to $\mathcal{S}$ is a realization of Equation (1) satisfying $(v(0), m(0)) = \mathcal{O}$, and there exists $\tau^* \in \mathbb{R}^+$ for which $(v(\tau^*), m(\tau^*))$ lies within the basin of attraction of $\mathcal{S}$ and for $\tau < \tau^*$, $(v(\tau), m(\tau))$ lies within the basin of attraction of $\mathcal{O}$. A similar defintion holds for tipping events from $\mathcal{S}$ to $\mathcal{O}$. The variable $\tau^*$ is itself a random variable and is referred to as the tipping time from $\mathcal{O}$ to $\mathcal{S}$. In Figures 3(a-b) we plot tipping events in the phase plane and as a time series. These numerical experiments indicate that $\mathcal{O}$ is far more susceptible to noise-induced tipping than $\mathcal{S}$. That is, the expected value of the tipping time from $\mathcal{O}$ to $\mathcal{S}$ is dramatically smaller than from $\mathcal{S}$ to $\mathcal{O}$. Moreover, noise-induced tipping events from $\mathcal{O}$ to $\mathcal{S}$ appear to be concentrated about a particular region in phase space.

The observations given above were quantitatively studied in the asymptotic limit $\sigma_1, \sigma_2 \to 0$

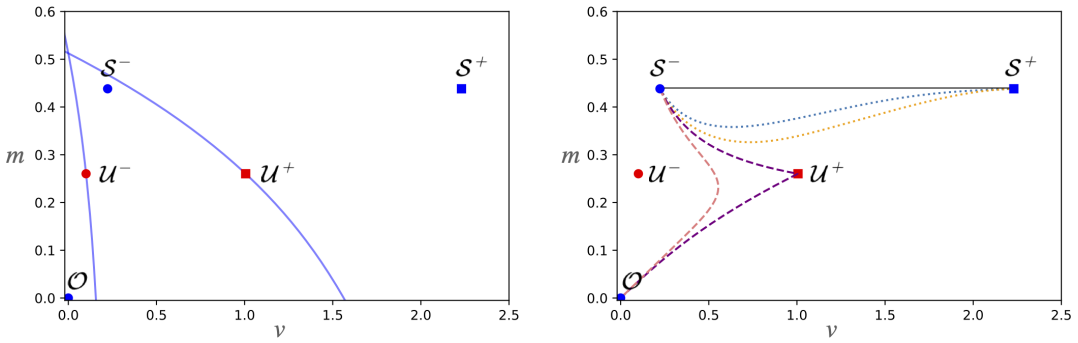


(a) (b)

Figure 2: The time-dependent functions are set as $\Lambda_r(\tau) = \frac{1}{2}(1 + \tanh(r\tau)), V_p(\tau) = 90\Lambda_r(\tau) + 10$, and $c(\tau) = 0.13V_p(\tau)$. The three fixed points at the start of the ramp, $\mathcal{O}$,$\mathcal{U}^-$,$\mathcal{S}^-$, and the three fixed points at the end of the ramp, $\mathcal{O}$,$\mathcal{U}^+$,$\mathcal{S}^+$ correspond to the non-storm state, the unstable storm state, and the stable storm state. (a) Blue curves correspond to the stable manifolds of $\mathcal{U}^-$ and $\mathcal{U}^+$. (b) Plot of the solutions of the time-dependent system for different values or $r$. The black curve is the solution when $r = 0$ and end-point tracks the stable path from $\mathcal{S}^-$ to $\mathcal{S}^+$. The blue and orange dotted curves correspond to solutions which end-point track the stable path from $\mathcal{S}^-$ to $\mathcal{S}^+$. The purple and pink dashed curves correspond to solutions which do not endpoint track the stable path, and tip from $\mathcal{S}^-$ to $\mathcal{O}$.

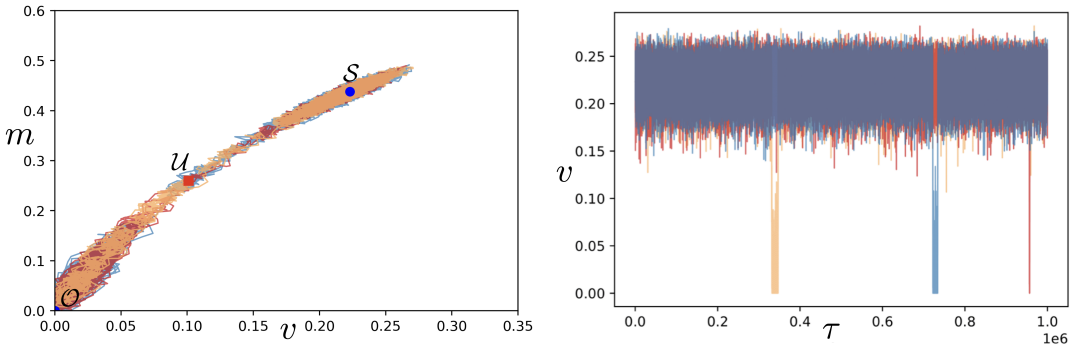


(a) (b)

Figure 3: Realizations of Equation (1) in phase space (a) and as a time series (b) for $\sigma_1 = \sigma_2 = 0.005, \gamma = 0.43$, $V_p = 10$, and $c = 0.286$.

using the Freidlin-Wentzell (FW) theory of large deviations; see [19–22] for thorough introductions to this topic. To simplify the following exposition, we let $F = (f, g)$ denote the vector field with components $f$, $g$, introduce the matrix

$$\Sigma = \begin{bmatrix} \sigma_1^{-2} & 0 \\ 0 & \sigma_2^{-2} \end{bmatrix},$$

and define for $\mathbf{v}_1, \mathbf{v}_2 \in \mathbb{R}^2$ the weighted inner product $\langle \mathbf{v}_1, \mathbf{v}_2 \rangle_\Sigma = \mathbf{v}_1^T \Sigma \mathbf{v}_2$ and the weighted norm $\|\mathbf{v}_2 - \mathbf{v}_1\|_\Sigma^2 = \langle \mathbf{v}_2 - \mathbf{v}_1, \mathbf{v}_2 - \mathbf{v}_1 \rangle_\Sigma$. One key result from FW theory is that in the limit $\sigma_1, \sigma_2 \to 0$ tipping events concentrate about most probable transition paths $\Psi^*(s) = (\psi_1^*(s), \psi_2^*(s))$ which

minimize a rate functional. Specifically, for Equation (1), the rate functional is for most probable transition paths from $\mathcal{O}$ to $\mathcal{S}$ is given by

$$I[\Psi] = \frac{1}{2}\int_{-\infty}^{\infty} \|\dot{\Psi} - F(\Psi)\|_{\Sigma}^2 ds, \tag{2}$$

which is defined for sufficiently regular curves satisfying $\lim_{s\to-\infty}\Psi(s) = \mathcal{O}$ and $\lim_{s\to\infty}\Psi(s) = \mathcal{S}$. Furthermore, knowledge of the most probable transition path allows computation of the expected tipping time through the relationship

$$\mathbb{E}[\tau^*] = \exp(I[\Psi^*])\left(C + O\left(\left\|\sqrt{\Sigma^{-1}}\right\|\right)\right), \tag{3}$$

where $C > 0$ is a constant.

To numerically compute minimizers, we used a gradient flow which matches well with Monte-Carlo simulations; see Figure 4. However, through a Legendre transformation $\mathbf{p} = \Sigma(\dot{\Psi} - F(\Psi))$ the Euler-Lagrange equations corresponding to $I$ can be expressed in the following Hamiltonian form

$$\begin{aligned} \dot{\Psi} &= F(\Psi) + \Sigma^{-1}\mathbf{p}, \\ \dot{\mathbf{p}} &= -\nabla F^T(\Psi)\mathbf{p}, \end{aligned} \tag{4}$$

with corresponding Hamiltonian $H = \frac{1}{2}\|\mathbf{p}\|_{\Sigma^{-1}}^2 + \langle F(\Psi), \mathbf{p}\rangle$. Consequently, most probable transition paths can be interpreted as heteroclinic orbits connecting $\mathcal{O}$ to $\mathcal{U}$ joined to a curve satisfying the deterministic dynamics from $\mathcal{U}$ to $\mathcal{S}$, i.e., $\dot{\Psi} = F(\Psi)$ and $\mathbf{p} = 0$. At $(\mathcal{O}, 0)$ there are one-dimensional unstable and stable manifolds $\mathcal{W}^U$ and $\mathcal{W}^S$ respectively as well as a a two-dimensional center manifold $\mathcal{W}^C$. We found that the heteroclinic orbit is given by $H^{-1}(0)\cap\mathcal{W}^C$ which locally agrees with the center manifold for the deterministic dynamics. Using knowledge of the most probable path, we obtained the following scaling law (up to logarithmic equivalence) for the tipping time $\tau_r$ from a neighborhood of $\mathcal{O}$ of characteristic size $r$:

$$\mathbb{E}[\tau_r^*] \asymp \exp(I[\Psi^*, \mathbf{p}^*]) \lesssim \exp\left(\frac{4}{3}\frac{r^3c^7}{\sigma_1^2} + \frac{36}{7}\frac{c}{\sigma_2^2}\left(\frac{r^3c^7}{\sigma_1^2}\right)^2\right), \tag{5}$$

This scaling law identifies the two dimensionless measures of noise strength $\tilde{\sigma}_1^2 = \sigma_1^2/c^7$ and $\tilde{\sigma}_2^2 = \sigma_2^2/c$ which control the tipping time. In particular, in Figure 3 the ratio $c^7/\sigma_1^2$ is $O(1)$ explaing why $\mathcal{O}$ is particulary susceptible to noise-induced tipping.

# 4 Final Comments

In our analysis of tipping in a tropical storm, we considered the various tipping mechanisms to be independent of each other. A natural question is how do various mechanisms couple to induce tipping events and so a natural extension of the analysis presented in our work is consider the interplay of a parameter shift and additive noise. For the specific system we considered, we expect that in tipping away from the stable storm state, there will be an interplay between the

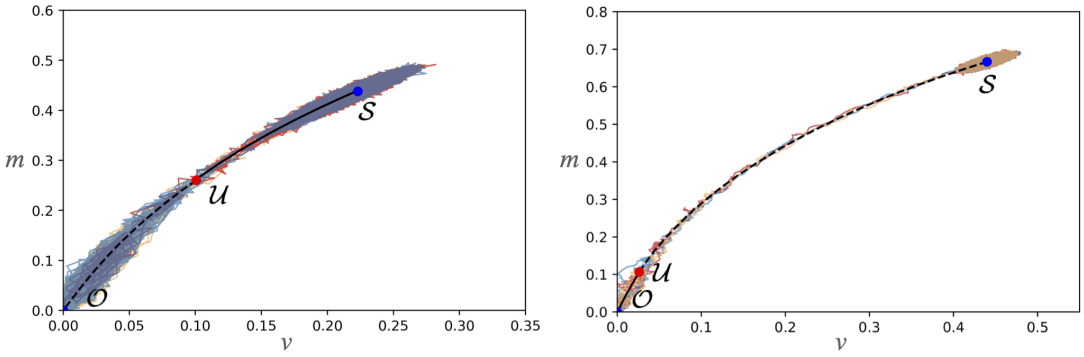


(a) (b)

Figure 4: Plots of the most probable path using a combination of the gradient flow and the deterministic dynamics, overlaid on tipping events. In each plot, the solid black curve represents the piece of the most probable path computing using a gradient flow and the dashed black curve represents the the path following the deterministic dynamics. Parameter values are set as $\sigma_1 = \sigma_2 = .005, \gamma = 0.43$, $V_p = 10$. (a) Most probable path from $\mathcal{S}$ to $\mathcal{O}$ for $c = 0.286$. (b) Most probable path from $\mathcal{S}$ to $\mathcal{O}$ for $c = 0.22$.

rate and noise-induced tipping mechanisms, and the additive noise will lower the critical rate needed for tipping [23, 24]. Additionally, tipping should occur away from the non-storm state, but as there was no rate-induced tipping with this initialization, we must explore how rapidly changing parameters could enhance or inhibit noise induced tipping from $\mathcal{O}$.

## References

[1] T. M. Lenton, J. Rockström, O. Gaffney, S. Rahmstorf, K. Richardson, W. Steffen, and H. J. Schellnhuber, "Climate tipping points—too risky to bet against," *Nature*, vol. 575, no. 7784, pp. 592–595, 2019.

[2] P. Ashwin, C. Perryman, and S. Wieczorek, "Parameter shifts for nonautonomous systems in low dimension: bifurcation-and rate-induced tipping," *Nonlinearity*, vol. 30, no. 6, p. 2185, 2017.

[3] P. Ashwin, S. Wieczorek, R. Vitolo, and P. Cox, "Tipping points in open systems: bifurcation, noise-induced and rate-dependent examples in the climate system," *Philosophical Transactions of the Royal Society A*, vol. 370, no. 1962, pp. 1166–1184, 2012.

[4] J. Thompson and J. Sieber, "Predicting climate tipping as a noisy bifurcation: a review," *International Journal of Bifurcation and Chaos*, vol. 21, no. 02, pp. 399–423, 2011.

[5] T. Lenton, "Early warning of climate tipping points," *Nature Climate Change*, vol. 1, no. 4, p. 201, 2011.

[6] L. Halekotte and U. Feudel, "Minimal fatal shocks in multistable complex networks," *Scientific reports*, vol. 10, no. 1, pp. 1–13, 2020.

[7] H. Alkhayuon, R. C. Tyson, and S. Wieczorek, "Phase tipping: how cyclic ecosystems respond to contemporary climate," *Proceedings of the Royal Society A*, vol. 477, no. 2254, p. 20210059, 2021.

[8] D. J. Wuebbles, D. W. Fahey, K. A. Hibbard, D. J. Dokken, B. C. Stewart, T. K. Maycock, D. J. Wuebbles, D. W. Fahey, K. A. Hibbard, B. DeAngelo, S. Doherty, K. Hayhoe, R. Horton, J. P. Kossin, P. C. Taylor, A. M. Waple, and C. P. Weaver, *Executive summary*, pp. 12–34. Washington, DC, USA: U.S. Global Change Research Program, 2017.

[9] K. Slyman, J. A. Gemmer, N. K. Corak, C. Kiers, and C. K. Jones, "Tipping in a low-dimensional model of a tropical cyclone," *Physica D: Nonlinear Phenomena*, vol. 457, p. 133969, 2024.

[10] N. Mori, T. Takemi, Y. Tachikawa, H. Tatano, T. Shimura, T. Tanaka, T. Fujimi, Y. Osakada, A. Webb, and E. Nakakita, "Recent nationwide climate change impact assessments of natural hazards in japan and east asia," *Weather and Climate Extremes*, vol. 32, p. 100309, 2021.

[11] C. Dahlgren and K. Sherman, "Preliminary assessment of hurricane dorian's impact on coral reefs of abaco and grand bahama," *Perry Institute of Marine Science Report to the Government of The Bahamas*, 2020.

[12] A. Graumann, T. G. Houston, J. H. Lawrimore, D. H. Levinson, N. Lott, S. McCown, S. Stephens, and D. B. Wuertz, "Hurricane katrina: A climatological perspective: Preliminary report," *US Department of Commerce, National Oceanic and Atmospheric Administration, National Environmental Satellite Data and Information Service, National Climatic Data Center*, 2006.

[13] K. Emanuel, "Hurricanes: Tempests in a greenhouse," *Physics Today*, vol. 59, no. 8, pp. 74–75, 2006.

[14] K. Emanuel, "Self-stratification of tropical cyclone outflow. part ii: Implications for storm intensification," *Journal of the Atmospheric Sciences*, vol. 69, no. 3, pp. 988 – 996, 2012.

[15] K. Emanuel and F. Zhang, "The role of inner-core moisture in tropical cyclone predictability and practical forecast skill," *Journal of the Atmospheric Sciences*, vol. 74, no. 7, pp. 2315–2324, 2017.

[16] K. Emanuel, "A fast intensity simulator for tropical cyclone risk analysis," *Natural Hazards*, vol. 88, pp. 779–796, Sept. 2017.

[17] S. Wieczorek, C. Xie, and P. Ashwin, "Rate-induced tipping: Thresholds, edge states and connecting orbits," *Nonlinearity*, vol. 36, no. 6, p. 3238, 2023.

[18] C. Kiers and C. K. Jones, "On conditions for rate-induced tipping in multi-dimensional dynamical systems," *Journal of Dynamics and Differential Equations*, vol. 32, pp. 483–503, 2020.

[19] M. I. Freidlin and A. D. Wentzell, *Random perturbations of dynamical systems*, vol. 260. Springer Science & Business Media, 2012.

[20] N. Berglund, "Kramers' law: Validity, derivations and generalisations," *Markov Process Relat Fields*, vol. 19, no. 3, pp. 459–490, 2013.

[21] E. Forgoston and R. O. Moore, "A primer on noise-induced transitions in applied dynamical systems," *SIAM Rev*, vol. 60, no. 4, pp. 969–1009, 2018.

[22] V. M. Gálfi, V. Lucarini, F. Ragone, and J. Wouters, "Applications of large deviation theory in geophysical fluid dynamics and climate science," *La Rivista del Nuovo Cimento*, vol. 44, no. 6, pp. 291–363, 2021.

[23] P. Ritchie and J. Sieber, "Early-warning indicators for rate-induced tipping," *Chaos: An Interdisciplinary Journal of Nonlinear Science*, vol. 26, no. 9, p. 093116, 2016.

[24] K. Slyman and C. K. Jones, "Rate and noise-induced tipping working in concert," *Chaos: An Interdisciplinary Journal of Nonlinear Science*, vol. 33, no. 1, 2023.